A novel mesh saliency approximation for polygonal mesh segmentation

Hung-Kuang Chen & Mu-Wei Li

Multimedia Tools and Applications
An International Journal

ISSN 1380-7501
Volume 77
Number 13

Multimed Tools Appl (2018)
77:17223-17246
DOI 10.1007/s11042-017-5287-4

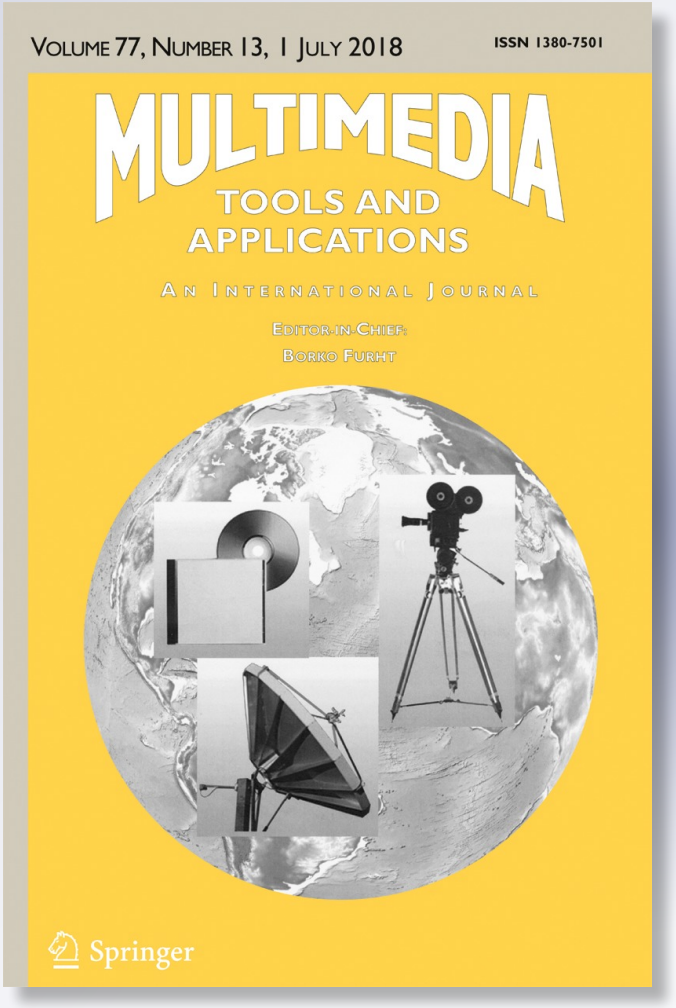

Springer

Multimed Tools Appl (2018) 77:17223–17246
https://doi.org/10.1007/s11042-017-5287-4

A novel mesh saliency approximation for polygonal mesh segmentation

Hung-Kuang Chen[1] · **Mu-Wei Li**[1]

Received: 13 March 2017 / Revised: 24 August 2017 / Accepted: 5 October 2017 /
Published online: 13 October 2017

Abstract To assist a great variety of applications including object recognition or shape matching, 3D scene analysis, view point selection, mesh simplification, segmentation, and 3D printing etc., the approximation of mesh or part saliency has been intensively studied in recent years. A recent trend on developing such techniques has been turned from utilizing local or global shape descriptors to human visual perceptual rules. Consequently, the concepts and the theories from cognition science were extensively applied. In this paper, we borrowed the theory of part salience by Hoffman and Singh and devised an approach to mesh or part saliency computations. Unlike previous attempts, we proposed a single scalable measure of mesh or part saliency via a linear combination of the three factors of human visual perception, i.e, the degree of part protrusion, the relative size of a part, and the strength of a part's boundaries, in addition to their individual quantizations. To verify the efficacy of our approach, an iterative saliency-optimized polygonal mesh segmentation is devised. To provide an objective quantitative evaluation in addition to traditional visual inspection, a public domain benchmark software developed by Chen et al. was deployed. According to the inspections on the colored segments and the benchmarking scores, our saliency computation indeed improves the segmentation of 3D objects with protrusive parts, outperforming a number of well-known approaches.

Keywords Mesh saliency · Part salience · Mesh segmentation

✉ Hung-Kuang Chen
hankchentw@gmail.com

Mu-Wei Li
zx1122337@gmail.com

[1] Electronic Engineering Department, National Chin-Yi University of Technology, Taichung 41170, Taiwan

1 Introduction

The study of perception inspired metrics to assist geometric processing of 3D Objects has drawn a considerable attention within these years [7, 9, 14, 15, 25, 28, 34, 41, 46, 47]. To effectively capture perceptually important regions on a 3D mesh, the measurement of *saliency* for three dimensional objects incorporating perceptual criteria with geometric properties is critical to the success of a great variety of applications including shape matching [9], view point selection [7, 25, 34], scan integration [41], mesh simplification [25, 28, 41, 47], mesh segmentation [41], and 3D printing [46].

Traditional techniques based on mathematical geometric measures such the curvatures and normals are mostly developed for CAD generated objects with extremely sharp features. With the significant advances in geometric modeling techniques, an increasing demand has been identified on human visual perception-based metrics. To understand a 3D shape and mimic the human vision, a theory of part salience was proposed by D. Hoffman et al. [14, 15]. According to his theory, human vision usually recognized or learned an object from its shapes by dissecting it into several visibly distinctive parts, where the *salience* of a part depends on (at least) three factors: the *relative part size*, the *degree of protrusion*, and the *boundary strength*. On the basis of such theory, a great number of techniques have been developed for mesh segmentation [1, 3, 18, 20, 23, 26, 30, 35, 44, 45, 49–52]. Most of these works considered the three factors individually; only a few of them have jointly dealt with these three factors.

For example, to give an estimation of the degree of protrusion, Lin et al. [30] suggested a discrete version of a continuous function μ for topology matching proposed by [12]. Unlike [12], Lin's integral function as follows is constructed from the dual graph of a given mesh $M(V, F)$ where V, F respectively represents the set of vertices and faces of M.

$$\mu(v) = \sum_i g(v, b_i) area(f_i), \forall v \in V \tag{1}$$

where b_i represents the dual-vertex of face $f_i \in F$. The protrusion degree of a vertex v is then estimated by a normalization of $\mu(v)$ as follows.

$$P(v) = \frac{(u(v) - u_{min})}{u_{max}}. \tag{2}$$

Since their approximation of protrusion degree requires an integral of geodesic distances, a significant amount of execution time spent on computing All-Pairs-Shortest-Paths [20, 30, 45]. In addition, to locate the boundary on concave creases and satisfy the minima rule, a sophisticated procedure tracing locale change is required.

To address this issue, we propose a simple and efficient measure of mesh, or part, saliency with respect to the three factors of part salience. Unlike previous attempts, we started with the quantizations of the three factors, i.e., protrusion degree, boundary strength, and relative part size, and derived a novel mesh, or part, salience measure by a linear weighted summation of the three quantized and normalized factors. To verify the efficacy of our approach to saliency calculation, a part-type mesh segmentation algorithm on the basis of such metric is proposed. In addition to traditional colored segments approach via human visual inspection, an objective quantitative evaluation using a public benchmark suit by Chen et al. is performed on the segmented results [6]. According to the experimental results, our saliency-optimized part-type mesh segmentation method not only outperforms the other well-known techniques at the benchmark scores but also excels the other methods in visual inspection.

2 Notations and terminologies

To facilitate our discussions, a number of basic notations and terminologies are summarized as follows.

We have assumed that the input object to be decomposed by our method is represented by an orientable 3D mesh denoted as $M = (V, E, F$, where V, E, F respectively represents a set of vertices defined in a three dimensional Cartesian space R^3, a set of edges, and a set of faces. In particular, we assume that all the faces are triangulated; thus each $f \in F$ has three vertices, e.g., $v_a, v_b, v_c \in V$, and three edges, i.e., $e_{a,b} = \overline{v_a v_b}$, $e_{b,c} = \overline{v_b v_c}$, $e_{c,a} = \overline{v_c v_a} \in E$. Furthermore, for a vertex $v \in V$, we denoted

1. $R(v)$ as the *ring* of v, representing the set faces adjacent to v,
2. $C(v)$ as the *crown* of v, representing the set vertices on the boundary of the ring of v.

This definition can be extended to k-ring neighbourhood of a vertex v by introducing the vertices and faces from k levels of BFS traversal. An example illustrating the 1-, 2-, and 3-ring neighborhoods of a vertex v is shown in the Fig. 1.

3 Related works

Prior to the discussion of our works, a number of related works are briefly reviewed in this section. According to the type and use of the related works, we began our review with a brief introduction to the theory of part salience and the works on mesh saliency, followed by a review of existing mesh segmentation methods based on the visual perceptual theories.

3.1 Part or mesh saliency

Hoffman and Richards [14] proposed a theory on object recognition for the human visual perception; in which, a rule, called the minima rule, was introduced for dividing a surface into parts. The minima rule suggests dividing an object(surface) into parts at loci of negative minima of each principal curvature, following the principle of *transversality*: a concave crease is formed at the locus of the intersection of two 3D shapes. In a later work, Braunstein et al. conducted three experiments to test such theory [5]. On the basis of the minima rule, a theory of visual part salience is proposed to evaluate the visual significance of the parts of an object, which claims that the visual salience of the parts was contributed to at least three factors [15]. Namely,

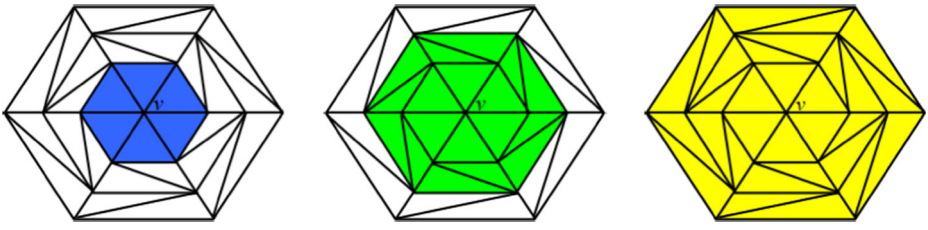

Fig. 1 The 1-, 2-, and 3-ring neighborhoods of a vertex v

1. the *degree of protrusion* measured by by the ratio of its surface area excluding its base(s) to the area of its base(s),
2. the *relative part size* defined as the ratio of the volume enclosed by the surfaces of the part to the volume of the entire object,
3. the *boundary strength* estimated by the mean turning angle or the maximum turning angle over the entire boundary.

The earliest study on the salience of 3D meshes, or the *mesh saliency*, using perceptual metric was started from the work by C.-H. Lee et al. [25]. In their work, they adopted the center-surround mechanism proposed by Itti et al. [17], originally developed for saliency computations of image pixels. In particular, they also demonstrate the use of the computed saliency information with mesh simplifications and salient view point selection.

Gal and Cohen-Or introduced a method for partial shape matching and similarity calculation using salient geometric features following the theory of salience of visual parts by Hoffman and Singh [15]. Quantitative measurement based on curvatures for the computation of the boundary strength was proposed. On the basis of such definitions, the salience of a part was then defined on the factors of relative size and the boundary strength.

Addressing on the problem of viewpoint selection, Feixas et al. proposed a unified framework for view-based mesh saliency computation. On the basis of the definition view point saliency, the most salient view can be determined to show the most salient part of an object [7]. A more recent work reported by Nouri et al. approached the problem by perceptual multi-scale salient map [34], i.e., using patches of adaptive size for local vertex descriptors, defining saliency as the vertices' degree, and aggregating the saliency information between different scales.

Wu et al. approached the problem of mesh saliency by proposing their set of metrics following two principles of visual saliency, i.e., the principles of local contrast and global rarity. The local mesh saliency is approximated by a multi-scale local descriptor measuring the dissimilarity between the vertices using various sizes of height maps and a local contrast measurement of the saliency of each surface patch by a weighted sum of contrast to neighboring patches. On the other hand, the global rarity measurement of a vertex is evaluated by its contrast to all the other vertices, i.e., costing $O(n^2)$.

By considering the properties of the log Laplacian spectrum of a 3D mesh, Song et al. developed a method for mesh saliency computation via spectral processing. They reported that the mesh saliency is highly related to the irregularity of the log-Laplacian spectrum of a 3D mesh. A number of classic applications of mesh saliency including saliency-guided simplification, segmentation, and scan integration were also presented. In a more recent work, Limper et al. approximating the mesh saliency using local curvature entropy. Their approach showed a significant improvement on the computation times comparing with other spectral based methods [28].

Recently, a study on measuring and validating the visual salience computations of 3D printed objects was proposed [46]. To analyze viewing behaviors, the fixations positions, or gaze locations, of a number of subjects are computed and gathered for validating the computational model of mesh saliency.

3.2 Mesh segmentation

Dissecting a three-dimensional object into components has been identified as an essential preprocessing tool in a variety of geometric modeling applications [38]. According to [37], the problem of 3D mesh segmentation can be defined as follows.

Definition 1 (Mesh Segmentation) Let $M(V, F)$ be an orientable 3D polygon mesh and V, F respectively represent the set of vertices and faces of M. An arbitrary segmentation of M, denoted as Σ, introduces a partition of M into k disjoint sub-sets $\{M_0, ..., M_{k-1}\}$ such that

$$\Sigma(M) = \{M_0, ..., M_{k-1}\} \tag{3}$$

Moreover, the problem of mesh segmentation can be further formulated as an optimization problem as follows.

Definition 2 (Mesh Segmentation Optimization) Given an orientable 3D polygon mesh M and a criterion function J defined on the segmentation of M under a set of constraints C, namely, $J : \Sigma(M) \rightarrow \mathbf{R}$. The set of optimal segmentations of M of minimum cost J_{min} with respect to the criterion function J is given by

$$\arg\min_{\Sigma(M)} J(\Sigma(M)), \tag{4}$$

where $J_{min} = J(\Sigma(M))$ is minimal.

Depending on the application, the type of the outcomes and the criterion function vary with the objectives of the segmentation. On the basis of such observation, a crude classification suggested by Ariel Shamir [38] broadly categorized existing segmentation methods into two general types: namely, *surface-type* or *part-type* segmentation. Part-type segmentation decomposes a 3-D object into a number of disjoint meaningful parts to facilitate subsequent processing such as texture mapping [27], modeling [8], morphing [11, 53], shape-based retrieval [54], and skeleton extraction [20], etc. By contrast, surface type segmentation partitions the input mesh into a set of non-overlapping patches. In this paper, only a limited number of relevant works were briefly reviewed. For a more comprehensive survey, the readers may refer to the studies presented in [4, 6, 24, 31, 33, 38, 42, 43]. The review of existing published literature is grouped according to their segmented results, i.e., parts or patches, as follows.

3.2.1 Part-type segmentation

On the basis of the observation of an analogy between the singularity in surface tangents and the singularity in electrostatics, Wu and Levine [48, 49] proposed a physically-based approach to segmenting the object into parts at deep surface concavities. Following the concept of minima rule, the deep surface concavities are detected by tracing the local minima of the charge density by simulating the charge density distribution over an object's surface.

Another approach, called *fuzzy clustering*, was proposed to hierarchically decompose a 3D mesh [20]. Their approach iteratively decomposes the input mesh into two opposing parts. The boundary between the two parts is optimized by performing a maximum-flow/minimum-cut with respect to a weighted combination of the geodesic and angular distances on the fuzzy region. The iteration stopped when a set of prescribed constraints such as the relative size or the number of parts is satisfied.

Zhang et al. [51] proposed another region growing algorithm according to the minima rule, which expands the initial region from its seed vertices to those surrounded by the concave creases. The final result of their algorithm is a set of volumetric parts whose boundaries lie on deep concavities.

Lee et al. [26] presented an intelligent scissoring operator for meshes focusing on finding the contours for cutting. This approach is built on the minima rule and part salience theory

from the cognitive theory that provides an aid to divide a surface mesh into visual meaningful parts along the concave creases and to determine the saliency of segments, respectively. Their approach is able to construct closed boundaries of the parts by applying an efficient shortest path algorithm over the open boundary of the mesh so that the boundary can be closed. Consequently, it may also create some parts that have low perceptually meaning.

Page et al. [35] introduced a new algorithm for mesh segmentation, called the Fast Marching Watersheds. Their new algorithm is based on a hill-climbing watershed algorithm that leveraged a heap structure to control the flooding across the mesh and the minima rule to decomposed the mesh into visual meaningful parts.

D. H. Kim et al. [21] proposed another shape decomposition scheme that recursively performs constrained morphological decomposition (CMD) to optimize decomposition. According to their experimental results, their scheme yields an intuitive description and provides robustness to scaling, rotation, noise, shape deformation, and occlusion.

Lin et al. proposed a quantitative approach [29, 30] to carry out the theory of part salience from cognitive science [15]. To evaluate the protrusion of a given part, they have adopted the continuous function $\mu(v)$ defined by an integral of the geodesic distances proposed by Hilaga et al. for Reeb Graph construction [12]. In a later work, Valette et al. [45] also applied the principle of the protrusion function to express the degree of closeness of a vertex to a protrusive part.

On the assumption of an object comprising a core body and a set of protrusive parts, Agathos et al. [1] proposed a segmentation algorithm similar to Lin's approach [29, 30]. On the basis of prominent feature extraction and core approximation, their method is able to decompose the input object into perceptually meaningful parts. Likewise, a minimum cut algorithm is also applied to trace the partitioning boundaries.

Kaick et al. [18] presented a shape segmentation method for complete and incomplete shapes by directly optimizing the decomposition according to the geometric characterization of the parts on the basis of an intermediate-level analysis. Instead of processing polygon meshes, it focused on the treatment of incomplete shapes in point clouds acquired by a range scanner.

3.2.2 Patch-type segmentation

Zhang et al. [52] considered decomposing compound objects via *Gaussian curvature analysis*. Their approach comprises three major steps: namely, the Gaussian curvature estimation, boundary detection, and region growing. Where the boundaries between two articulated parts with highly negative curvature are identified based on the theory of *transversality*.

Emanoil Zuckerberger et al. addressed the problem of decomposing a polyhedral surface into "meaningful" patches and proposed two segmentation algorithms applying *flooding convex decomposition* and *watershed decomposition* targeting on content-based retrieval, metamorphosis and simplification of three-dimensional models [54].

Shymon Shlafman et al. proposed a general framework for producing morph sequences that maintained the distinctive features of the input models [40]; it combined an algorithm for decomposing surfaces into patches and an algorithm for morphing polyhedral surfaces by projecting cylinder-like patches based on the observations that human visual system tends to segment complex objects at regions of matched concavities. Given a user-specified number of segments, k, their decomposition algorithm begins with the selection of a set of k seed faces followed by iteratively assigning faces to the closest clusters followed by an iteration of assigning and adjusting the seeds to make it lying at the center of the assigned cluster. The iteration stopped its execution until such assignments and adjustments were converges.

To locate concave creases and seams, Au et al. [3] presented an automatic mesh segmentation algorithm exploiting shape concavities using a set of concavity-sensitive scalar fields computed by a Laplacian system solver with concavity-sensitive weights. The computed scalar fields are then used to evaluate the candidate cuts by employing a score-based greedy algorithm.

3.3 Benchmarks for mesh segmentation

Recently, a number of works have been developed to provide quantitative evaluations on existing mesh segmentation algorithms; instead of presenting qualitative results as coloured segments, a public standard established upon a set of objective metrics were proposed [2, 4, 6, 31, 43].

Attene et al. [2] compared five segmentation algorithms on eleven 3D surface meshes. However, their evaluation and comparison merely qualitative, showing side-by-side images of colored segments. Xiaobai Chen et al. at Princeton University proposed a benchmark comprising 4,300 manually generated segmentations for 380 surface meshes [6]. Their benchmark provided four quantitative metrics analyzing 11 geometric properties of the segmentations of 19 different object categories. Since their benchmark software was adopted in our evaluation of the segmentation algorithm, the computing evaluation metrics produced from their benchmark are briefly reviewed as follows.

3.3.1 Cut discrepancy

Cut Discrepancy(CD) sums the distances from points along the boundary of a segment to the closest ones from the boundary of corresponding ground truth segment, and vice-versa [16]. Assuming C_1 and C_2 are sets of all points on the segment boundaries of segmentations S_1 and S_2, respectively, and $dG(p_1, p_2) = \min\{d_G(p_1, p_2), \forall p_2 \in C_2\}$ measures the geodesic distance between two points on a mesh. The Directional Cut Discrepancy, $DCD(S_1 \implies S_2) = mean\{d_G(p_1, C_2), \forall p_1 \in C_1\}$, is defined as the mean of the distribution of $d_G(p_1, C_2)$ for all points $p_1 \in C_1$. The Cut Discrepancy,

$$CD(S_1, S_2) = \frac{DCD(S_1 \implies S_2) + DCD(S_2 \implies S_1)}{avgRadius}, \tag{5}$$

is defined to be the mean of the directional functions in both directions divided by the average Euclidean distance from a point on the surface to the center of the mesh, denoted as $avgRadius$.

3.3.2 Hamming distance

Hamming Distance(HD) measures the overall regional differences between two segmented meshes [16]. Given two mesh segmentation $S^1 = S_1^1, S_1^2, \cdots, S_1^m$ and $S^2 = S_2^1, S_2^2, \cdots, S_2^m$ with m and n segments, respectively, the Directional Hamming Distance is defined as

$$DH(S_1 \implies S_2) = \sum_i \| S_2^i \setminus S_1^{\max_k \| S_2^i \cap S_1^k \|} \|. \tag{6}$$

3.3.3 Rand index

Rand Index(RI) measures the likelihood that a pair of faces is in the same segment in two segmentations or not [36]. Assuming $S1$ and $S2$ as two segmentations, s_1^i and s_2^i as the segment IDs of face i in S_1 and S_2, and N as the number of faces in the polygonal mesh, $C_{ij} = 1 \iff s_1^i = s_1^j$, and $P_{ij} = 1 \iff s_2^i = s_2^j$. The Rand Index is defined as follows

$$RI(S_1, S_2) = \binom{2}{N}^{-1} \sum_{i,j,i<j} [C_{ij} P_{ij} + (1 - C_{ij})(1 - P_{ij})] \tag{7}$$

3.3.4 Consistency error

Consistency Error(CE) account for nested, hierarchical similarities and differences in segmentations [32]. Assuming $R(S, f)$ is a segment in a segmentation S comprising a face f. The local refinement error is defined as

$$E(S_1, S_2, f) = \frac{\|R(S_1, f) \setminus R(S_2, f_i)\|}{\|R(S_1, f)\|}, \tag{8}$$

where n is the number of faces in the polygon mesh model.

Given the refinement error of each face $f \in F$, the Global Consistency Error (GCE) and Local Consistency Error (LCE) metrics were defined as follows.

$$GCE(S_1, S_2, f) = \frac{1}{n} \min\{\sum_i E(S_1, S_2, f_i), \sum_i E(S_2, S_1, f_i)\} \tag{9}$$

$$LCE(S_1, S_2, f) = \frac{1}{n} \sum_i \min\{E(S_1, S_2, f_i), E(S_2, S_1, f_i)\} \tag{10}$$

To evaluate and compare the results of automatic segmentation algorithms, seven well-known algorithms was tested, i.e., the K-Means by Shlafman et al. [40], the Random walks by Lai et al. [22], Fitting Primitives by Attene et al. [2], Normalized cuts by Golovinskiy et al. [10], Randomized cuts by Golovinskiy et al. [10], Core extraction by Katz et al. [19], and Shape Diameter Function by Shapira et al. [39]. All of them, except the K-Means, were performed with its original implementation using the default parameters.

4 Our mesh or part saliency approximation

Unlike previous works, our approach approximates the part saliency by a weighted linear combination of the three factors suggested by Hoffman et al. [15] instead of considering them individually.

4.1 The protrusion degree

Unlike Lin's approach [30], our definition of protrusion degree is defined on each vertex of the mesh rather than on the dual vertex of a triangle face. Furthermore, the estimation can be considered as an extension of the protrusion measure of a 2D shape given by Hoffman et al. [15]. Hence, it is more intuitive than those proposed in [1, 13, 30].

The protrusion degree of a vertex v with respect to its $k-$ring neighborhood, $R_k(v)$, is defined as follows.

Let $c_0(v) = v$, the geometric center of the k-crown of v is given by

$$c_i(v) = \frac{1}{\|C_i(v)\|} \sum_{\forall v_j \in C_i(v)} v_j, i = 1, 2, \cdots k. \tag{11}$$

Note that $\|C_i(v)\|$ denotes the cardinality of the k-crown of vertex v. The protrusion degree of a vertex $v \in V$, denoted as $PD(v)$, defining on its k-ring neighborhood is given as follows.

$$PD(v) = \frac{\sum_{i=0}^{k} c_i c_{i+1}}{\max\limits_{v_i, v_j \in C_k(v)} \{\|\overline{v_i v_j}\|\}}. \tag{12}$$

Similar to (2), the value of protrusion degree can be normalized to the range [0,1].

4.2 The relative part size

Our measurement of the relative part size, denoted as $RS(M_i)$ is the ratio of the area of the submesh M_i to the area of the input mesh M. Hence, for a submesh M_i, the relative part size is given by

$$RS(M_i) = \frac{\sum\limits_{\forall f \in M_i} Area(f)}{\sum\limits_{\forall f \in M} Area(f)}, \tag{13}$$

which is essentially in the range of [0, 1].

4.3 The boundary strength

Since the saliency of a part boundary increases at convex and concave regions, we adopted the traditional dihedral angle approach for the determination of boundary strength. To illustrate this concept, an example is shown in Fig. 2. Assuming $e_{i,j}$ to be a boundary edge of a submesh M_k whose neighboring faces and their corresponding face normals are $\{f_i, f_j\}$ and $\{N_i, N_j\}$, respectively.

Let us denote the set of boundary edges of M_k as ∂M_k. The boundary strength of a part defined by M_k, denoted as $BS(M_k)$, is as follows.

$$BS(M_k) = \frac{\sum_{\forall e_{i,j} \in \partial M_k} \frac{1 - N_i \cdot N_j}{2}}{\|\partial M_k\|}, \tag{14}$$

where $\|\partial M_k\|$ is the cardinality of ∂M_k.

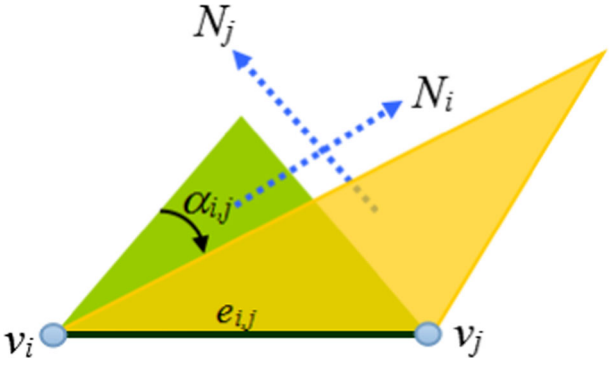

Fig. 2 The dihedral angle $\alpha_{i,j}$ defined on the edge $e_{i,j}$

4.4 The part saliency

To allow an overall optimization with respect to all the three factors at once, the saliency of a part, $PS(M_i)$, consisted of a local mesh M_i is defined as a linear weighted sum of (12), (13) and (14). Namely,

$$PS(M_i) = \alpha \cdot PD(M_i) + \beta \cdot RS(M_i) + \gamma \cdot BS(M_i), \tag{15}$$

where α, β, and γ, are constant weights. Specifically, we may confine these three weights by requiring $\alpha + \beta + \gamma = 1$ if the three factors are properly normalized and scaled to the range [0, 1].

The vertex saliency of $v \in V$, denoted as $s = VS(R(v))$, can be computed from (15) with respect to the ring neighbourhood of a vertex $v \in V$, or $R(v)$. A possible way to visualize the saliency information of a mesh is to assign vertex colors as follows.

$$Color(s) = (1-s)^2 \times R + 2s(1-s) \times G + s^2 \times B. \tag{16}$$

Note that the colors of red, green, blue are denoted as R, G, and B, respectively. As an example, the Armadillo mesh rendered according to (16) is shown in Fig. 3.

Apparently, the tips of protrusive parts in Fig. 3 are red or reddish, which implied higher saliency values relative to the other regions; hence, it is particularly useful in identifying protrusive parts. Furthermore, such measurement can be applied to a versatile of applications including polygonal mesh segmentation, simplification, compression, matching, and watermarking.

5 Part-type segmentation using our mesh saliency approximation

As an example, we will show how our approximation of mesh saliency can be applied for polygonal mesh segmentation in the following section. Following Definition 2, we may treat our segmentation problem as an optimization problem maximizing the mesh saliency

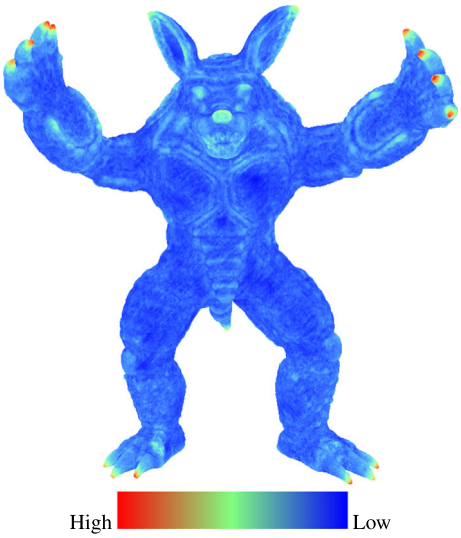

Fig. 3 The distribution of the vertex saliency of Armadillo mesh determined by our part saliency approximation.

with respect to our saliency function $PS(\Sigma(M))$. Namely, the problem of segmentation optimization is revised as follows.

Definition 3 (Mesh Saliency Optimized Segmentation) Given an orientable 3D polygon mesh M and a saliency function PS defined on the segmentation of M under a set of constraints I. The set of optimal segmentations of M of maximum saliency PS_{max} with respect to the saliency function PS is given by

$$\arg\max_{\Sigma(M)} PS(\Sigma(M)), \tag{17}$$

where $PS_{max} = \arg\max_{\Sigma(M)} PS(\Sigma(M))$ is maximal.

To obtain an approximation of $\Sigma(M) = \{M_0, M_1, \cdots, M_{i-1}\}$, the segmentation begins with the search of a set of salient features $C = \{c_0, c_1, \cdots, c_{i-1}\}$ derived from our saliency approximation given in (15); on the basis of these features, an optimal decomposition of M^i can be computed by applying saliency-optimized region growing from the features. The growing process eventually stopped at a set of parts, $\Sigma_C(M) = \{M_0, M_1, \cdots, M_{i-1}\}$, that satisfies

$$\arg\max_{C} PS(\Sigma_C(M)) = \arg\max_{C}(PS(M_0) + PS(M_1) + \cdots + PS(M_{i-1})) \tag{18}$$

In summary, our algorithm iteratively executes the following stages to yield a nearly optimal segmentations of M with respect to the saliency function S .

1. Salient features computation.
2. Salient representative determination.
3. Saliency optimized region growing.
4. Boundary determination and smoothing.

The four stages are performed iteratively until one of a set of prescribe constraints such as the threshold of relative part size, maximum number of segments, iteration depth, etc., is satisfied.

5.1 Salient features computation

According to (12), the length of the part defined by the 3-ring neighborhood of the vertex v is given by the path length $\|\overline{c_0c_1c_2c_3}\|$ and the width of its base is $\|\overline{v_{3,1}v_{3,5}}\|$. Consequently, in this case, the protrusion degree is

$$PD(v) = \frac{\sum_{i=0}^{2}\|\overline{c_ic_{i+1}}\|}{\max\limits_{v_i,v_j\in\partial R_3(v)}\{\|\overline{v_iv_j}\|\}}. \tag{19}$$

On the basis of (19), (14) and (13), the vertex saliency of a vertex v with respect to its k-ring neighborhood $R_k(v)$ is given as follows.

$$VS(v) = \alpha PD(R_k(v)) + \beta BS(R_k(v)) + \gamma RS(R_k(v)). \tag{20}$$

Note that, such a measure combining three multi-scale local shape descriptors is itself a perceptual multi-scale saliency metric. On the basis such metric, a number of feature points are then selected from a check for their regional optimality. Figure 4a–d shows a number of objects and their feature points in green dots.

The representative feature is then iteratively selected from the unsegmented region by applying the following approach called the *fast opposite face selection*(FSFS).

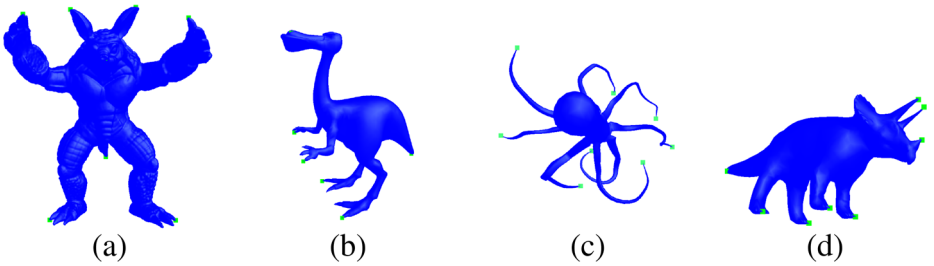

Fig. 4 The feature points of a number of example meshes determined according to our saliency approximation: **a** the Armadillo mesh; **b** the Dinopet mesh; **c** the Octpus mesh; **d** the Triceratops mesh

5.2 Salient representative determination

To bipartite the input mesh, Katz et al. [20] used a modified version of All-Pairs-Shortest-Paths(APSP) to evaluate the weighted distances between each pair of features. Two points with longest weighted distance in the candidate set are selected as the initial features. However, such approach takes $O(\binom{m}{2}n^2 \log n) = O(m^2 n^2 \log n)$ for an input mesh of n vertices and m initial features. Instead of applying APSP, we proposed a quicker and yet more effective approach called the *fast opposite face selection*(FSFS).

Given an arbitrary pair of feature points in C, e.g., v_a and v_b, as well as the center of the input mesh, O, we approximate the distance $D(v_a, v_b)$ between any pair of features, v_a and v_b, by the perimeter of the triangle $T(v_a, v_b, O)$ as follows.

$$D(v_a, v_b) = \|\overline{v_a v_b}\| + \|\overline{v_b O}\| + \|\overline{O v_a}\| \tag{21}$$

Two opposite features are then determined by applying Algorithm 1.

Algorithm 1 Fast Opposite Features Selection

Require: $C = \emptyset$;
Require: L, left feature point;
Require: R, right feature point;
Require: S_T, vertex saliency threshold;
Require: $D_{max} = 0$, maximum distance between opposite features;

for all $v \in V$ **do**
  if $(S(v) > S_T)$ **and** $(S(v) = \max_{\forall v_j \in R^3(v)} \{S(v_j)\})$ **then**
    $C = C \bigcup \{v\}$;
  end if
end for
for all $v_i \in C$ **do**
  $L \leftarrow v_i$
  for all $v_j \in C, j > i$ **do**
    if $(D(v_i, v_j) > D_{max})$ **then**
      $D_{max} \leftarrow D(v_i, v_j)$
      $R \leftarrow v_j$
    end if
  end for
end for

As an example, the two opposite feature points with longest weighted distance found by applying Algorithm 1 to the Armadillo mesh are indicated by a line connecting them in Fig. 5.

To grow a part, the feature with higher saliency is then selected as the seed for subsequent region growing process.

5.3 Saliency optimized region growing

To distinguish high curvature parts from the low curvature ones, the relative part size is an accumulation of a combination of gauss areas and common surface areas during region growing. In this context, surface area and gauss area of a triangle face $T(v_a, v_b, v_c)$ are respectively denoted as $A_S(T)$ and $A_G(T)$. According to the Gauss-Bonnet theorem, the gauss area $A_G(T)$ is determined by the area of a spherical patch on the surface of a unit sphere in vector space mapped from the normal vectors of its three vertices, namely, N_a, N_b, and N_c. The spherical triangle spanned by these three normal vectors are called *Euler triangle* and its area can be calculated by

$$A_G(t) = \alpha + \beta + \gamma - \pi \tag{22}$$

where α, β, and γ are its interior angles.

The effective area A_E can then be approximated by a combination of surface area A_S and Gauss area $A_G$with a heuristic weights δ providing adaptive control, i.e.,

$$A_E(t) = \delta \times A_S(T_i) + (1 - \delta)A_G(T_i) \tag{23}$$

In each step, the growing process is proceeded by a BFS traversal over the current part P, which is denoted as $BFS(P)$; from which, a set of candidate faces, C_f is constructed. To optimize the saliency of current part, a triangle t is not inserted to the current part P if the saliency of P is decreased after the insertion of t; on the contrary, t is accepted for insertion to P provided that the saliency is increased after the insertion. The process is repeated until

Fig. 5 The two opposite features of the Armadillo mesh determined by the two farthest feature points with the largest distance D

the saliency of the current part reaches a maximal S_max, i.e., the first local maximal. We detailed the process of the saliency optimized region growing with Algorithm 2 shown as follows.

Algorithm 2 Region Growing

Require: M, the input mesh;
Require: P, the part mesh;
Require: C, the set of candidate faces;
Require: PR_{min}, the minimum relative part size;
Require: $level$, the level of iteration;
Require: f, a temporary holder for a face;
Require: v_{seed}, the initial feature points;
Require: $UpdFlag$, a flag variable;

$C \leftarrow v_{seed}$
$UpdFlag \leftarrow$ **FALSE**
repeat
  $C \leftarrow BFS(C)$
  for all $f \in C$ **do**
    if $((S(P \cup \{f\}) > S(P))$ **then**
      $P \leftarrow (P \cup f)$
      $UpdFlag \leftarrow$ **TRUE**
    end if
  end for
until $(UpdFlag =$ **FALSE**$)$ **and** $RS(P) \geq PR_{min}$
return P

An example showing such process is given in the Fig. 6.

5.3.1 Boundary determination and smoothing

In comparison with most previous works relying solely on the minima rule, the boundary determination in our work relied on the control of saliency variation during the region growing process. Namely, a boundary is formed on the edges of a part when the insertion of adjacent triangles reduces the part saliency. However, the resulted boundaries between adjacent parts may have a jaggy outlook, which is not desirable for most subsequent geometric processing. Therefore, a smoothing process is usually required. In this work, we followed the minimum cut approach by Katz et al. [20]. A fuzzy region can be created for such process by expanding current boundaries from three to five more levels of BFS traversal. Figure 7 gives an example of the results.

6 Experimental results

In this section, we will present our experimental results with respect to three aspects, namely, the runtime efficiency, objective quantitative analysis, and subjective visual inspection. To verify our idea, we adopted the benchmark suit by Xiaobai Chen et al. [6] from Princeton University to provide quantitative analysis over the segmented meshes produced from our work by comparing with those from manual decomposition and a number of well-known automatic mesh segmentation algorithms. However, not all the test meshes are

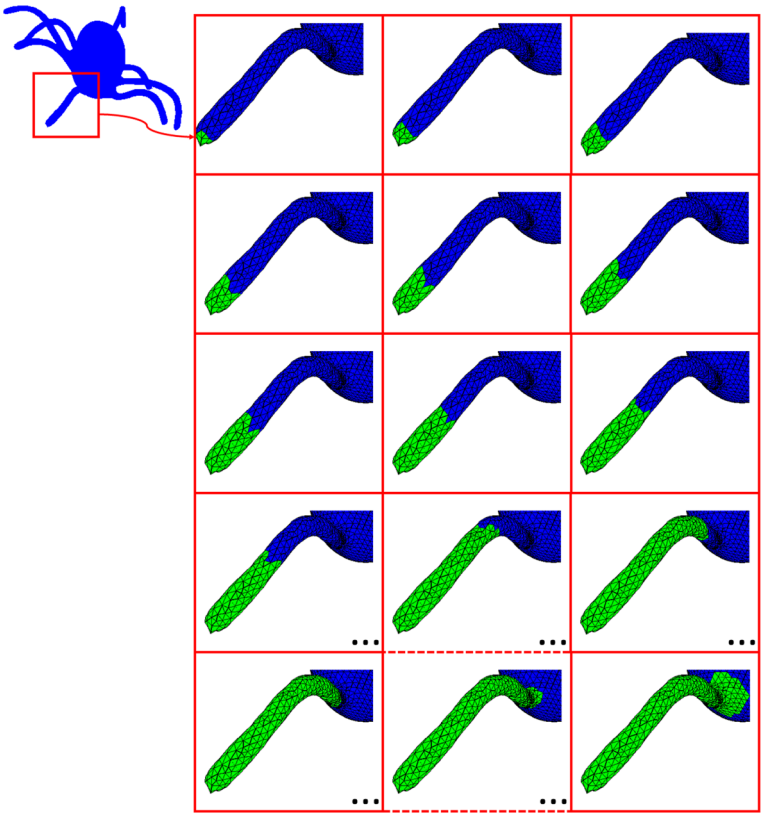

Fig. 6 An example of determining a part by our region growing: the growing process stopped at the dashed frame

Fig. 7 The determined boundary(left) and its smoothed result(right)

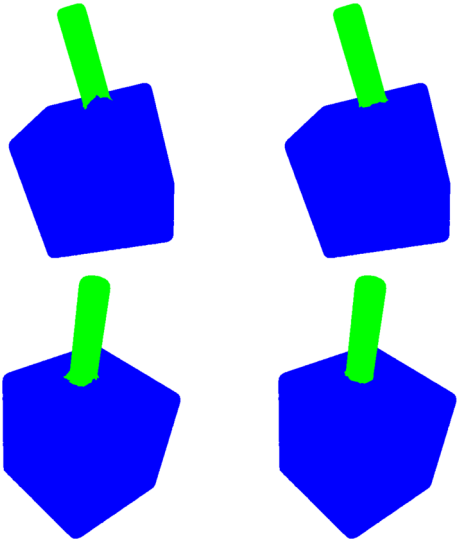

Table 1 The attributes and processing time of all the models used in our experiments

Mesh	$\|V\|$	$\|F\|$	No. of Segs.	Ex. Times(secs.)
Human	11015	22026	6	4.2
Cup	15136	30268	2	4.0
Glasses	7420	14836	4	4.8
Airplane	5109	10214	7	1.0
Ant	7038	14072	11	7.3
Octopus	10466	20932	9	2.7
Table	10100	20196	5	2.0
Teddy	13324	26644	7	5.3
Hand	7242	14480	7	2.6
Plier	4487	8970	5	1.3
Fish	6076	12148	5	2.1
Bird	3714	7424	7	1.2
Armadill	25494	50984	9	14.8
Mech	15505	31006	2	4.1
Bearing	14956	29924	2	6.8
Vase	9356	18708	3	3.4
Fourleg	8411	16818	9	3.4

adopted in our experiments; instead, only a subset of the experimental meshes that have protrusive parts are adopted. All the experiments were performed on a PC with Intel Core i5-4430 processor, 8GB RAM, and an NVIDIA GeForce GT 640 powered display card.

6.1 Runtime efficiency

The runtime efficiency of our segmentation algorithm is evaluated by program running times. A summary of our test results is summarized in Table 1. The statistics of each test mesh along with their processing time are listed in Table 1 shown as follows.

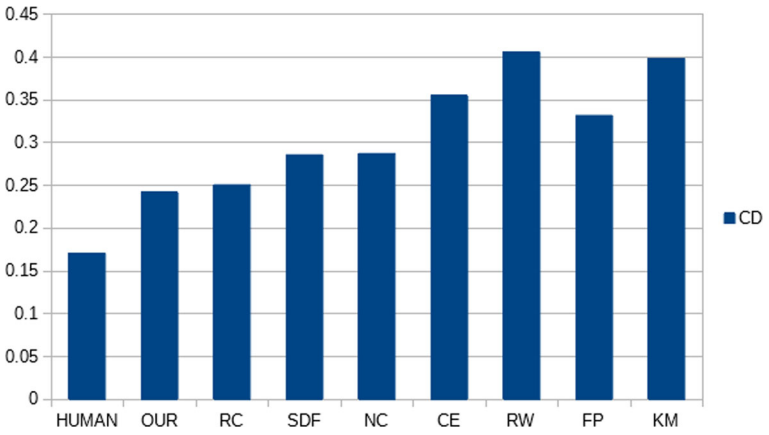

Fig. 8 Cut Discrepancy

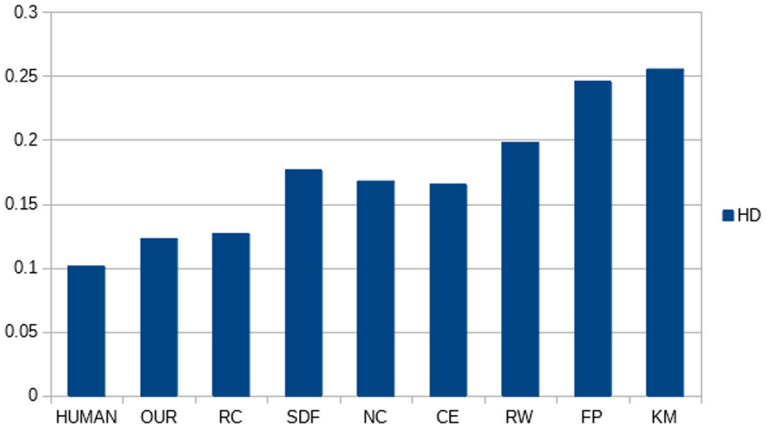

Fig. 9 Hamming Distance

6.2 Quantitative analysis

To show the efficacy of our approach, the public benchmark suite developed by Xiaobai Chen et al. [6] from Princeton University was adopted to give an objective quantitative evaluation. In the benchmark tests, four metrics, namely, the Cut Discrepancy(CD), Hamming Distance(HD), Rand index(RI), and Consistency Error(CE), were used.

The quantitative evaluations in terms of the testing scores are performed by comparing our scores with seven existing methods including the K-Means(KM) by Shlafman et al. [40], the Random Walks(RW) by Lai et al. [22], Fitting Primitives(FP) by Attene et al. [2], Normalized Cuts(NC) by Golovinskiy et al. [10], Randomized Cuts(RC) by Golovinskiy et al. [10], Core Extraction(CE) by Katz et al. [19], and Shape Diameter Function(SDF) by Shapira et al. [39]. For comparison, the statistical charts of test scores calculated from the benchmark software based on the metrics of Cut Discrepancy, Hamming Distance, Random Index, and Consistency Error are presented in Figs. 8, 9, 10 and 11, respectively.

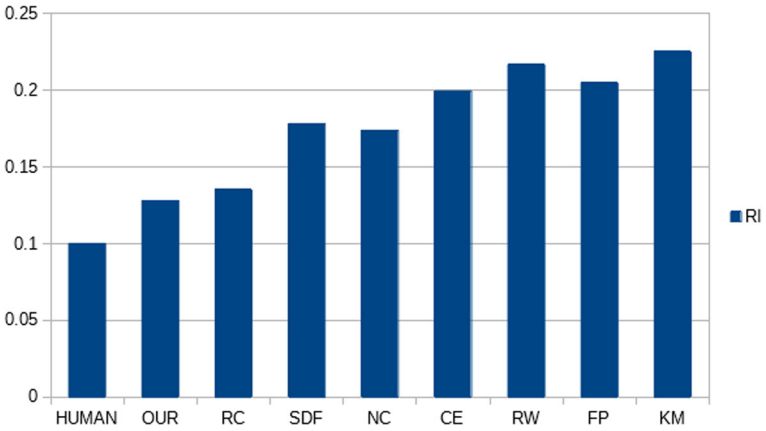

Fig. 10 Rand Index

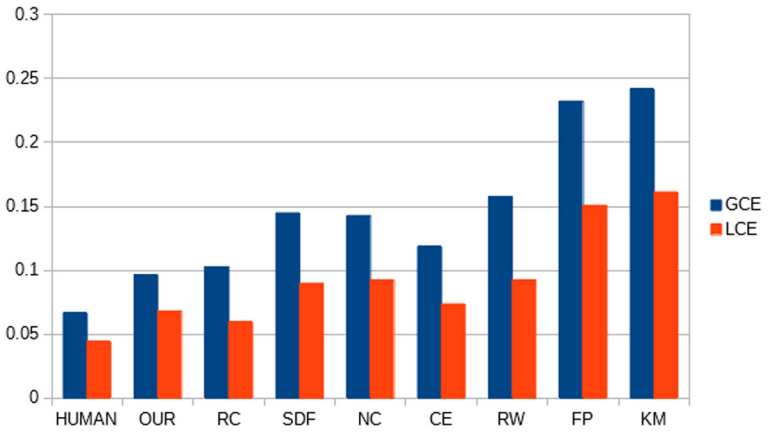

Fig. 11 Consistency Error

6.2.1 Cut discrepancy

The scores running with the metrics of Cut Discrepancy, defined as the mean of the directional functions in both directions divided by the average Euclidean distance from a point on the surface to the centroid of the mesh [16], is presented with the chart in Fig. 8.

According to comparison presented in Fig. 8, the error of the segmented results from our algorithm measured with Cut Discrepancy metric is lower than the other methods and is very close to the result of Random Cut.

6.2.2 Hamming distance

The results using Hamming Distance(HD) measure for overall regional differences between the segmented meshes by the methods of evaluation and Human are presented in Fig. 9.

From the results shown in Fig. 9, the errors of our segmentation in Hamming Distance deviated from the human created segmentation, 'HUMAN', is also lower than the others.

6.2.3 Rand index

To measures the likelihood of a pair of faces in the same segment of two segmentations, namely, the segmented meshes of evaluated and 'Human' approaches, the metric of Cut Discrepancy is applied. Associated results are presented in Fig. 10.

According to Fig. 10, our algorithm still outperforms the other methods.

6.2.4 Consistency error

The results on Consistency Error(CE), measuring nested, hierarchical similarities and differences between the evaluated and 'Human' segmentations, are shown in Fig. 11.

According to Fig. 11, the Random Cut(RC), Shape Diameter Function(SDF), and our methods have very close scores in Global Consistency Error(GCE); by contrast, the Local Consistency Error(LCE) of our method is slightly higher than those of the RC and SDF methods.

In summary, the test scores presented in Figs. 8, 9, 10 and 11 confirmed that our method can be successfully applied at mesh segmentation.

6.3 Visual inspections

According to the results presented in the last subsection, our method is competitive with the methods running Randomized Cuts [10] and Shape Diameter Function [39]. Hence, in this

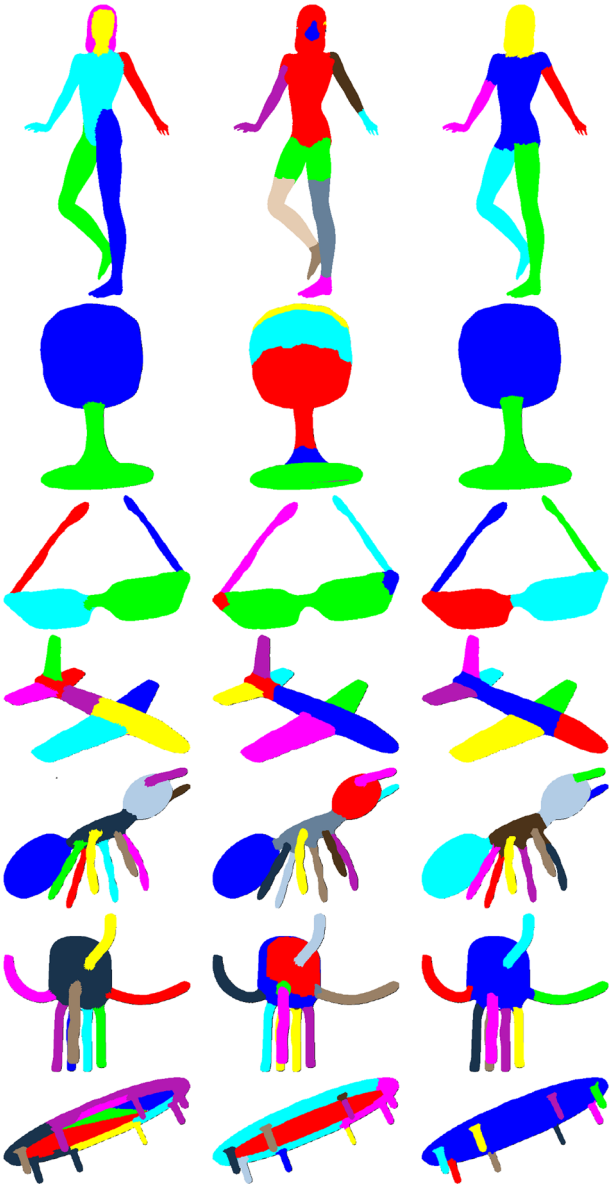

Fig. 12 The segmentation results of the Human, Cup, Glasses, Airplane, Ant, Octopus, and Table meshes by the Randomized Cuts(left), Shape Diameter Function(middle), and our method(right)

section, a number of segmented meshes resulted from the two methods are compared with ours. The comparisons using coloured segmented meshes are presented in Figs. 12 and 13. In order to distinguish the subtle differences visually, all of the segments are in different colour. Figure 12 shows the results of segmented Human, Cup, Glasses, Airplane, Ant,

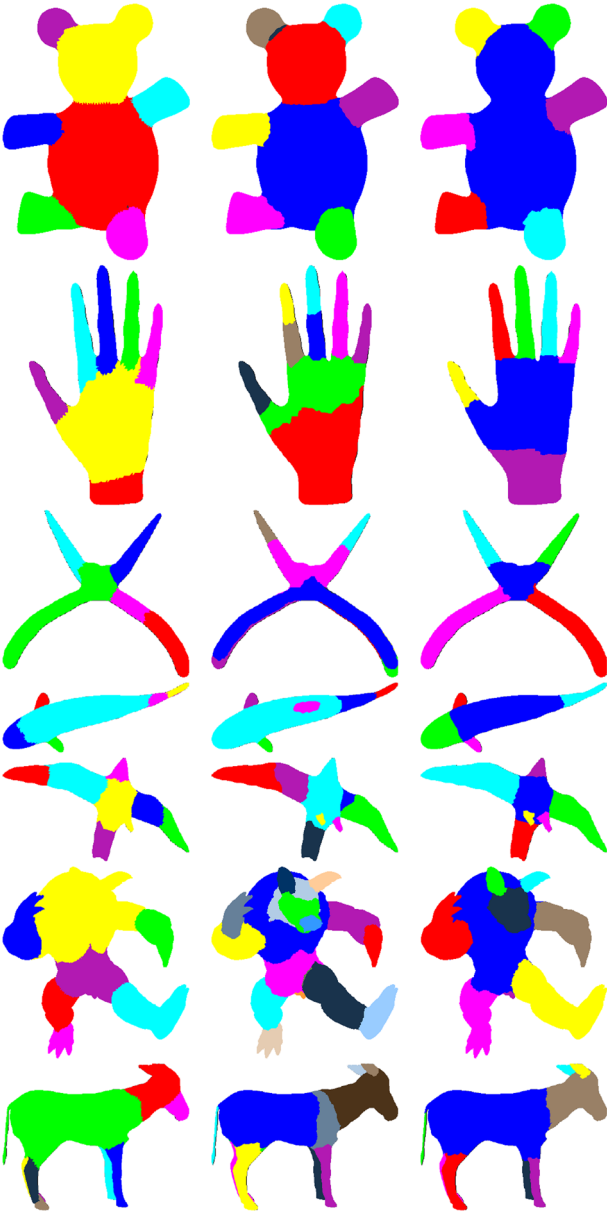

Fig. 13 The segmentation results by the Randomized Cuts(left), Shape Diameter Function(middle), and our method(right)

Octopus, and Table meshes using the Randomized Cuts, Shape Diameter Function, and our method.

By inspecting the segmented results of the Human mesh, it is very clear to see than an over segmentation problem occurred in the SDF version, yet an under segmentation problems can be found on the right shoulder and left leg of the RC version. By contrast, both kinds of problems were not found in our version; the head and limbs are properly separated from the torso. Note that, over segmentation is observed on the SDF version of Cup, Glasses, Airplane, Octopus and Table meshes, the RC version of Airplane and Table meshes.

In addition, the segmented results of Teddy, Hand, Plier, Fish, Bird, Armadillo, and Fourleg meshes are presented in Fig. 13.

The over segmentation problem occurred in the SDF-version of the ear of Teddy, Hand, Plier, Fish, Bird, and Fourlegs meshes, the RC version of Plier and Fish meshes. On the other hand, under segmentation problems are identified in the SDF-version Plier and Armadillo meshes. As for the other meshes in Fig. 13, the parts are segmented properly according to the minima rule by locating the part boundaries at concave creases.

7 Concluding remarks and future works

Unlike existing works, we propose a multi-scale approach to the approximation of saliency of a mesh or part based on the theory borrowed from cognitive science [5, 15]. Compared with traditional local shape metrics, e.g., the curvature, our saliency approximation has the benefits of combining multi-scale local and global shape features including the protrusion degree, relative size, and boundary strength. To verify our approach, a novel mesh segmentation method using saliency-optimized region growing is proposed. Objective and subjective evaluations in terms of a public domain benchmark by Chen et al. [6] and colored segmented meshes respectively were performed on a subset of meshes from Chen's [6] benchmark. According to the results presented in this paper, the proposed approach to 3D mesh segmentation using our novel mesh saliency approximation obviously outperforms the existing methods and matches with the theory of human visual perception.

In summary, our novel approach has at least the following contributions:

1. A comprehensive and adaptive approximation to the saliency of a polygonal mesh that integrates the three factors of part saliency.
2. An efficient fully automatic part-type mesh segmentation algorithm featuring low time-complexity and high quality-outputs that matched with human cognitive theory.

Moreover, with the advent of our novel opposite feature selection method, the time complexity of initial feature calculation has significantly reduced from $O(m^2 \times n^2 \log n)$ to $O(m^2)$ provided that the number of features is m. With the novel region growing control scheme considering both surface area and guass area, the region grows faster in the flat area but is slower in curved region. As a result, the segmented result matches with human vision.

However, the proposed segmentation algorithm still has its limitations. For those objects without protrusive parts, concave and convex creases, e.g., a sphere, our method cannot identify high saliency feature points for its uniformity of saliency values. This may restrict the application of our approach. Under such circumstances, traditional patch-type methods may work much better than ours.

Acknowledgements We would like to thank Xiaobai Chen, Aleksey Golovinskiy, and Thomas Funkhouser in Princeton University for their benchmark software and associated test meshes.

References

1. Agathos A, Pratikakis I, Perantonis SJ, Sapidis NS (2010) Protrusion-oriented 3d mesh segmentation. Vis Comput 26(1):63–81. https://doi.org/10.1007/s00371-009-0383-8
2. Attene M, Falcidieno B, Spagnuolo M (2006) Hierarchical mesh segmentation based on fitting primitives. Vis Comput 22(3):181–193. https://doi.org/10.1007/s00371-006-0375-x
3. Au OC, Zheng Y, Chen M, Xu P, Tai CL (2012) Mesh segmentation with concavity-aware fields. IEEE Trans Vis Comput Graph 18(7):1125–1134. https://doi.org/10.1109/TVCG.2011.131
4. Benhabiles H, Vandeborre JP, Lavoué G, Daoudi M (2010) A comparative study of existing metrics for 3d-mesh segmentation evaluation. Vis Comput 26(12):1451–1466. https://doi.org/10.1007/s00371-010-0494-2
5. Braunstein ML, Hoffman DD, Saidpour A (1989) Parts of visual objects: An experimental test of the minima rule. Perception 18(6):817–826. https://doi.org/10.1068/p180817. PMID: 2628932
6. Chen X, Golovinskiy A, Funkhouser T (2009) A benchmark for 3d mesh segmentation. ACM Trans Graph 28(3):73:1–73:12. https://doi.org/10.1145/1531326.1531379
7. Feixas M, Sbert M, González F (2009) A unified information-theoretic framework for viewpoint selection and mesh saliency. ACM Trans Appl Percept 6(1):1:1–1:23. https://doi.org/10.1145/1462055.1462056
8. Funkhouser T, Kazhdan M, Shilane P, Min P, Kiefer W, Tal A, Rusinkiewicz S, Dobkin D (2004) Modeling by example. ACM Trans Graph 23(3):652–663. https://doi.org/10.1145/1015706.1015775
9. Gal R, Cohen-Or D (2006) Salient geometric features for partial shape matching and similarity. ACM Trans Graph 25(1):130–150. https://doi.org/10.1145/1122501.1122507
10. Golovinskiy A, Funkhouser T (2008) Randomized cuts for 3d mesh analysis. ACM Trans Graph 27(5):145:1–145:12. https://doi.org/10.1145/1409060.1409098
11. Gregory A, Lin MC, Manocha D, Livingston MA et al (1999) Interactive surface decomposition for polyhedral morphing. Vis Comput 15(9):453–470
12. Hilaga M, Shinagawa Y, Kohmura T, Kunii TL (2001) Topology matching for fully automatic similarity estimation of 3d shapes. In: Proceedings of the 28th annual conference on computer graphics and interactive techniques, SIGGRAPH '01. ACM, New York, pp 203–212. https://doi.org/10.1145/383259.383282
13. Ho TC, Chuang JH (2012) Volume based mesh segmentation. J Inf Sci Eng 28(4):705–722
14. Hoffman D, Richards W (1984) Parts of recognition. Cognition 18(1):65–96 https://doi.org/10.1016/0010-0277(84)90022-2. http://www.sciencedirect.com/science/article/pii/0010027784900222
15. Hoffman DD, Singh M (1997) Salience of visual parts. Cognition 63(1):29–78 https://doi.org/10.1016/S0010-0277(96)00791-3. http://www.sciencedirect.com/science/article/pii/S0010027796007913
16. Huang Q, Dom B (1995) Quantitative methods of evaluating image segmentation. In: Proceedings., international conference on image processing, vol 3, pp 53–56. https://doi.org/10.1109/ICIP.1995.537578
17. Itti L, Koch C, Niebur E (1998) A model of saliency-based visual attention for rapid scene analysis. IEEE Trans Pattern Anal Mach Intell 20(11):1254–1259. https://doi.org/10.1109/34.730558
18. Kaick OV, Fish N, Kleiman Y, Asafi S, Cohen-OR D. (2014) Shape segmentation by approximate convexity analysis. ACM Trans Graph 34(1):4:1–4:11. https://doi.org/10.1145/2611811
19. Katz S, Leifman G, Tal A (2005) Mesh segmentation using feature point and core extraction. Vis Comput 21(8-10):649–658
20. Katz S, Tal A (2003) Hierarchical mesh decomposition using fuzzy clustering and cuts. ACM Trans Graph 22(3):954–961. https://doi.org/10.1145/882262.882369
21. Kim DH, Yun ID, Lee SU (2005) A new shape decomposition scheme for graph-based representation. Pattern Recogn 38(5):673–689. https://doi.org/10.1016/j.patcog.2004.10.003
22. Lai YK, Hu SM, Martin RR, Rosin PL (2008) Fast mesh segmentation using random walks. In: Proceedings of the 2008 ACM symposium on solid and physical modeling, SPM '08. ACM, New York, pp 183–191. https://doi.org/10.1145/1364901.1364927
23. Lavoué G, Dupont F, Baskurt A (2005) A new CAD mesh segmentation method, based on curvature tensor analysis. Comput Aided Des 37(10):975–987. https://doi.org/10.1016/j.cad.2004.09.001
24. Lavoué G, Vandeborre JP, Benhabiles H, Daoudi M, Huebner K, Mortara M, Spagnuolo M (2012) Shrec'12 track: 3d mesh segmentation. In: Proceedings of the 5th eurographics conference on 3d object retrieval, EG 3DOR'12. Eurographics Association, Aire-la-Ville, pp 93–99. https://doi.org/10.2312/3DOR/3DOR12/093-099
25. Lee CH, Varshney A, Jacobs DW (2005) Mesh saliency. ACM Trans Graph 24(3):659–666. https://doi.org/10.1145/1073204.1073244
26. Lee Y, Lee S, Shamir A, Cohen-Or D, Seidel HP (2005) Mesh scissoring with minima rule and part salience. Comput Aided Geom Des 22(5):444–465. https://doi.org/10.1016/j.cagd.2005.04.002
27. Lévy B., Petitjean S, Ray N, Maillot J (2002) Least squares conformal maps for automatic texture atlas generation. ACM Trans Graph 21(3):362–371. https://doi.org/10.1145/566654.566590

28. Limper M, Kuijper A, Fellner DW (2016) Mesh saliency analysis via local curvature entropy. In: Proceedings of the 37th annual conference of the european association for computer graphics: Short papers, EG '16. Eurographics Association, Goslar, pp 13–16. https://doi.org/10.2312/egsh.20161003
29. Lin HYS, Liao HY, Lin JC (2004) Visual salience-guided mesh decomposition. In: 2004 IEEE 6th workshop on Multimedia signal processing, pp 331–334. https://doi.org/10.1109/MMSP.2004.1436560
30. Lin HYS, Liao HY, Lin JC (2007) Visual salience-guided mesh decomposition. IEEE Trans Multimedia 9(1):46–57. https://doi.org/10.1109/TMM.2006.886344
31. Liu Z, Tang S, Bu S, Zhang H (2013) Smi 2013: New evaluation metrics for mesh segmentation. Comput Graph 37(6):553–564. https://doi.org/10.1016/j.cag.2013.05.021
32. Martin D, Fowlkes C, Tal D, Malik J (2001) A database of human segmented natural images and its application to evaluating segmentation algorithms and measuring ecological statistics. In: Proceedings eighth IEEE international conference on computer vision. ICCV 2001, vol 2, pp 416–423. https://doi.org/10.1109/ICCV.2001.937655
33. Meng M, Fan L, Liu L (2011) Smi 2011: Full paper: A comparative evaluation of foreground/background sketch-based mesh segmentation algorithms. Comput Graph 35(3):650–660. https://doi.org/10.1016/j.cag.2011.03.038
34. Nouri A, Charrier C, Lézoray O (2015) Multi-scale mesh saliency with local adaptive patches for view point selection. Signal Process Image Commun 38:151–166 https://doi.org/10.1016/j.image.2015.08.002. http://www.sciencedirect.com/science/article/pii/S0923596515001277. Recent Advances in Saliency Models, Applications and Evaluations
35. Page DL, Koschan A, Abidi MA (2003) Perception-based 3d triangle mesh segmentation using fast marching watersheds. In: 2003 IEEE computer society conference on Computer vision and pattern recognition, 2003. Proceedings, vol 2. IEEE eXpress Conference Publishing, Piscataway, pp 27–32. https://doi.org/10.1109/CVPR.2003.1211448
36. Rand WM (1971) Objective criteria for the evaluation of clustering methods. J Am Stat Assoc 66(336):846–850. https://doi.org/10.1080/01621459.1971.10482356
37. Shamir A (2004) A formulation of boundary mesh segmentation. In: Proceedings. 2nd international symposium on 3d data processing, visualization and transmission, 2004. 3DPVT 2004, pp 82–89, https://doi.org/10.1109/TDPVT.2004.1335163
38. Shamir A (2008) A survey on mesh segmentation techniques. Comput Graph Forum 27(6):1539–1556. https://doi.org/10.1111/j.1467-8659.2007.01103.x
39. Shapira L, Shamir A, Cohen-Or D (2008) Consistent mesh partitioning and skeletonisation using the shape diameter function. Vis Comput 24(4):249–259
40. Shlafman S, Tal A, Katz S (2002) Metamorphosis of polyhedral surfaces using decomposition. Comput Graph Forum 21(3):219–228. https://doi.org/10.1111/1467-8659.00581
41. Song R, Liu Y, Martin RR, Rosin PL (2014) Mesh saliency via spectral processing. ACM Trans Graph 33(1):6:1–6:17. https://doi.org/10.1145/2530691
42. Sun Xp, Wang L, Wang X, Zhao X (2015) A novel quantitative evaluation metric of 3d mesh segmentation. In: Park Jjjh, Pan Y, Chao HC, Yi G (eds) Ubiquitous Computing Application and Wireless Sensor, Lecture Notes in Electrical Engineering, vol 331. Springer, Netherlands, pp 621–628
43. Theologou P, Pratikakis I, Theoharis T (2015) A comprehensive overview of methodologies and performance evaluation frameworks in 3d mesh segmentation. Comput Vis Image Underst 135(0):49–82. https://doi.org/10.1016/j.cviu.2014.12.008. http://www.sciencedirect.com/science/article/pii/S1077314215000028
44. Tsuchie S, Higashi M (2014) Surface Mesh Segmentation and Reconstruction with Smooth Boundary Curves. In: Keyser J, Kim YJ, Wonka P (eds) Pacific graphics short papers. The eurographics association. https://doi.org/10.2312/pgs.20141247
45. Valette S, Kompatsiaris I, Strintzis MG (2005) A polygonal mesh partitioning algorithm based on protrusion conquest for perceptual 3d shape description. In: Workshop towards semantic virtual environments SVE 2005. Villars, Switzerland, pp 68–76
46. Wang X, Lindlbauer D, Lessig C, Maertens M, Alexa M (2016) Measuring the visual salience of 3d printed objects. IEEE Comput Graph Appl 36(4):46–55. https://doi.org/10.1109/MCG.2016.47
47. Wu J, Shen X, Zhu W, Liu L (2013) Mesh saliency with global rarity. Graph Model 75(5):255–264. https://doi.org/10.1016/j.gmod.2013.05.002. http://www.sciencedirect.com/science/article/pii/S1524070313000180
48. Wu K, Levine MD (1996) 3d part segmentation using simulated electrical charge distributions. In: Proceedings of 13th international conference on pattern recognition, vol 1, pp 14–18. https://doi.org/10.1109/ICPR.1996.545983
49. Wu K, Levine MD (1997) 3d part segmentation using simulated electrical charge distributions. IEEE Trans Pattern Anal Mach Intell 19(11):1223–1235. https://doi.org/10.1109/34.632982

50. Yan DM, Wang W, Liu Y, Yang Z (2012) Variational mesh segmentation via quadric surface fitting. Comput Aided Des 44(11):1072–1082. https://doi.org/10.1016/j.cad.2012.04.005. http://www.sciencedirect.com/science/article/pii/S0010448512000887
51. Zhang H, Liu R (2005) Mesh segmentation via recursive and visually salient spectral cuts. In: Proceedings of vision, modeling, and visualization. Citeseer, pp 429–436
52. Zhang Y, Paik J, Koschan A, Abidi M, Gorsich D (2002) Simple and efficient algorithm for part decomposition of 3-d triangulated models based on curvature analysis. In: 2002 international conference on Image processing. 2002. Proceedings, vol 3, pp III–273–III–276. https://doi.org/10.1109/ICIP.2002.1038958
53. Zöckler M., Stalling D, Hege HC (2000) Fast and intuitive generation of geometric shape transitions. Vis Comput 16(5):241–253
54. Zuckerberger E, Tal A, Shlafman S (2002) Polyhedral surface decomposition with applications. Comput Graph 26(5):733–743. https://doi.org/10.1016/S0097-8493(02)00128-0. http://www.sciencedirect.com/science/article/pii/S0097849302001280

Hung-Kuang Chen received his Ph.D. degrees in computer science of electronic engineering from National Taiwan University of Science and Technology, Taipei, Taiwan, in 1995 and 2006. From August 1995 to July 2002, he served as a Lecturer at the Department of Electronic Engineering of Lung-Hwa University of Science and technology, Taoyuan, Taiwan. From August 2002 to January 2007, he was a faculty of the Department of Information and Design of Asia University. Since February 2007, he served as an associate professor in the electronic engineering department of the National Chin-Yi University of Technology, Taichung, Taiwan. His research interests cover the computer graphics, virtual reality, and parallel computing.

Mu-Wei Li received his Bachelor degree of Engineering from the Department of Electronic Engineering of National Chin-Yi University of Science and Technology, Taipei, Taiwan, in 2015. Currently, he is pursuiting his Master degree of Engineering from the Department of Electronic Engineering of National Chin-Yi University of Science and Technology, Taipei, Taiwan. His research interests cover digital image processing, computer graphics, virtual reality, and computer game.